Article:
Timilsina, Sharad, Maharjan, Asim, Maharjan, Rijan et al. (2026) Photon-recycling lensless fluorometer. Journal of the Optical Society of America B: Optical Physics. B127-B131. ISSN: 0740-3224

https://doi.org/10.1364/JOSAB.588579

Research Article Vol. 43, No. 8 / August 2026 / Journal of the Optical Society of America B B127

Journal of the Optical Society of America B

OPTICAL PHYSICS

Photon-recycling lensless fluorometer

Sharad Timilsina,[1] Asim Maharjan,[1] Rijan Maharjan,[1,*] Rajin Pradhan,[1] Paru H. Rai,[1] Emiliano R. Martins,[2] Thomas F. Krauss,[3] and Ashim Dhakal[1]

[1]Biophotonics Laboratory, Phutung Research Institute, Tarakeshwar-7, Kathmandu 44611, Nepal
[2]Department of Electrical and Computer Engineering, University of São Paulo, São Paulo 13566-590, Brazil
[3]Department of Physics, University of York, York YO10 5DD, UK
*rm@pinstitute.org

Received 23 December 2025; revised 25 March 2026; accepted 16 April 2026; posted 23 April 2026; published 7 May 2026

Fluorometers typically employ multiple lenses and a single-pass optical geometry. We present a lensless fluorometer with a simple reflective sample chamber to recycle the unused excitation photons by reflecting them back into the sample volume while simultaneously redirecting emission photons toward the detector, thereby significantly enhancing the signal. By using commonly available aluminum bars, we experimentally achieve a 4.3× signal enhancement compared to a single-pass chamber in a lensless configuration. Combined with the documented 2× advantage of lensless systems, this design is projected to outperform standard lensed fluorometers by more than 8×. The enhanced performance allows for an 8× reduction in the excitation power while maintaining the required sub-parts-per-billion detection limit for tryptophan-like-fluorescence in drinking water. The power reduction significantly simplifies thermal and power management, which is essential for in-field and future handheld operation. We present a theoretical analysis that is supported by experimental results to validate this approach. Our system demonstrates a highly sensitive, power-efficient, and simplified platform for fluorescence measurement, opening new avenues for handheld and remote water quality sensing.

https://doi.org/10.1364/JOSAB.588579

1. INTRODUCTION

The standard methods for assessing fecal contamination in drinking water rely on quantifying thermo-tolerant coliforms (TTCs), including *Escherichia coli* (*E. coli*), using culturing techniques. Although accurate, these tests require specialized equipment, trained personnel, and have a long turnaround time of 12 to 48 h. To overcome these limitations, optical methods such as fluorescence spectroscopy and fluorometry are being investigated for the rapid quantification of microbial contamination. Many studies [1–3] have demonstrated a strong correlation between tryptophan-like fluorescence (TLF) (excitation/emission peaks ∼280/350 nm) and TTC levels. This suggests that measuring TLF intensity can serve as a rapid and robust indicator of fecal contamination in drinking water. Furthermore, these optical methods provide real-time results without requiring chemical reagents, and they utilize low-cost components, making them particularly well suited for resource-limited settings.

Typical fluorometers utilize lenses to focus the excitation light from a source onto the sample and to focus the resultant emitted fluorescence signal onto an optical detector. In our recent work, however, we demonstrated that for extended light sources (such as LEDs) and detectors, removing the lenses significantly increases the effective interaction volume, which, in turn, enhances the intensity of the collected fluorescence signal [4]. As a result, we were able to experimentally show that a lensless fluorometer collects twice the fluorescence signal compared to a similar lensed system.

Leveraging this lensless optical geometry, we incorporate a reflective material, specifically aluminum, for the sample chamber construction [Fig. 1(a)]. This design facilitates multiple passes for the excitation light, essentially recycling excitation photons that would otherwise be lost [Fig. 1(b)] in a single-pass geometry, thereby enhancing the effective interaction length. We demonstrate, both theoretically and experimentally, that with this "photon-recycling" sample chamber made from a commonly available 6061-T6 aluminum bar stock, the fluorescence signal can be further enhanced by a factor of 4.3, leading to an overall signal enhancement of >8 times compared to a lensed system.

Prior approaches have proposed the use of specialized optics, such as parabolic mirrors [5], mirror-coated cuvettes [6], and total internal reflection prisms [6], to achieve signal enhancement through multiple light passes. These solutions have already shown the promise of the photon-recycling approach, but they were developed in the context of beam paths determined by traditional lensed systems, use polished and protected

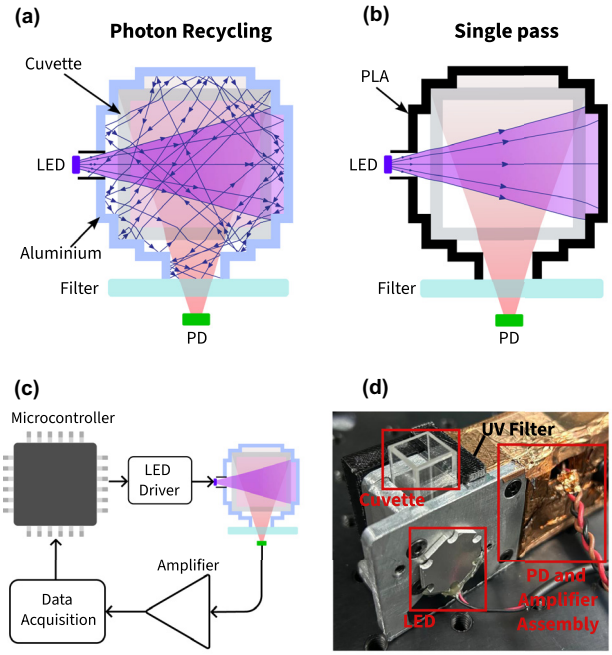

Fig. 1. Schematic representation of (a) photon-recycling and (b) single-pass sample chamber. (c) A block diagram representation and (d) an actual photograph of the experimental setup.

mirrors, and are not necessarily compatible with our low-cost vision.

Crucially, our lensless design eliminates the need for any specialized optical elements. Instead, we simply employ a cuvette chamber constructed from a common aluminum bar, which features two holes for the LED and the detector (see Fig. 1). A standard 3.5 mL quartz cuvette is placed inside this chamber to hold the sample. The excitation light therefore undergoes multiple reflection events within the aluminum chamber until it is either completely absorbed or exits through the light source/detector apertures, similar to an integrating sphere.

2. THEORETICAL MODEL

The total fluorescence flux Φ_{DET} received by the detector for a given excitation flux from the LED Φ_{LED} in a single-pass lensless system is proportional to the effective interaction length l_0, the fluorescence cross-section σ, and the number density of the fluorophores ρ [4]:

$$\Phi_{\mathrm{DET},0} = \frac{\Phi_{\mathrm{LED}}}{6}\rho\sigma l_0. \tag{1}$$

For a single-pass system, the effective interaction length l_0 is defined as [4]

$$l_0 = \frac{1}{A_{\mathrm{LED}}}\int_{V_C} F_{\mathrm{LED}}(\vec{r})\,F_{\mathrm{DET}}(\vec{r})\,\mathrm{d}V_C, \tag{2}$$

where $F_{\mathrm{LED}}(\vec{r})$ and $F_{\mathrm{DET}}(\vec{r})$, are the view-factors (i.e., flux transfer ratios) from the LED and the detector, respectively, and A_{LED} is the emission area of the detector. Please note that the integral is the effective volume for the system.

If the same cuvette system is completely enclosed in a photon-recycling chamber with walls of reflectivity R, the contribution in the effective interaction length from the nth reflection is given by $l_0(\mathrm{Re}^{-\alpha l_0\rho})^n$, with $e^{-\alpha l_0\rho}$ as the extinction factor due to fluorophore absorption (with molar absorption coefficient α) for each reflection. Unlike traditional integrating spheres, the initial unreflected fluorescence in our configuration represents a major component of the total detected signal. Due to the inherent non-uniformity of the rectangular reflective surfaces, our model focuses on the total flux incident on the detector, as characterized by the effective interaction length. The total effective interaction length for the reflective chamber l_R of the photon-recycling chamber is the sum of all possible reflections, given by

$$l_R = l_0 + l_0\mathrm{Re}^{-\alpha l_0\rho} + l_0(\mathrm{Re}^{-\alpha l_0\rho})^2 + \cdots + l_0(\mathrm{Re}^{-\alpha l_0\rho})^n + \cdots, \tag{3}$$

$$l_R = l_0\sum_{n=0}^{\infty}\left(\mathrm{Re}^{-\alpha l_0\rho}\right)^n = l_0\frac{1}{1-\mathrm{Re}^{-\alpha l_0\rho}}. \tag{4}$$

Note that the $\frac{1}{6}$ prefactor in Eq. (1) accounts for the fact that the signal is collected by the detector from one of the six sides of an infinitesimally small cuboid volume inside of the sample [4]. In a photon-recycling system, however, the detector also collects flux from the opposite side opposite due to reflection. We modify Eq. (1) to account for the reflected fluorescence flux collected by the detector:

$$\Phi_{\mathrm{DET},R} = \frac{\Phi_{\mathrm{LED}}}{6}\rho\sigma l_R + R\frac{\Phi_{\mathrm{LED}}}{6}\rho\sigma l_R = \frac{\Phi_{\mathrm{LED}}}{6}\rho\sigma l_R(1+R). \tag{5}$$

Thus, the fluorescence signal is enhanced by an enhancement factor Γ defined as

$$\Gamma = \frac{\Phi_{\mathrm{DET},R}}{\Phi_{\mathrm{DET},0}} = \frac{1+R}{1-\mathrm{Re}^{-\alpha l_0\rho}}. \tag{6}$$

So far, we have only considered the losses due to imperfect mirrors. The losses due to source/detector apertures in the chamber can be accounted for by a geometric factor ϵ, defined as the ratio of the actual reflecting surface area (without the apertures) to the total area (with the apertures) that receive the fluorescence flux. The geometric factor ϵ acts to decrease the overall reflectivity of all the reflecting surfaces—resulting in average reflectivity of ϵR—when considering the path length contribution multiple reflections [Eq. (3)]. Replacing R by ϵR in Eq. (3), we arrive at the enhancement factor as follows:

$$\Gamma_\epsilon = \frac{(1+R)}{1-\epsilon\mathrm{Re}^{-\alpha l_0\rho}}. \tag{7}$$

Note that ϵ is not present in the numerator, as the reflecting flux is entirely contributed by the opposite reflecting surface, which has no apertures.

3. THEORETICAL RESULTS

Let us consider a 100 ppb tryptophan (204.23 g/mol) sample, which has a molar absorption coefficient 5500 $\mathrm{M}^{-1}\,\mathrm{cm}^{-1}$ near 280 nm [7]. For an upper limit of interaction length $l_0 = 1$ cm (cuvette path length), the absorbance $\alpha l_0\rho \approx 2.7\times10^{-3}$ implying $e^{-\alpha l_0\rho} \approx 1$. Therefore, for typical concentrations with

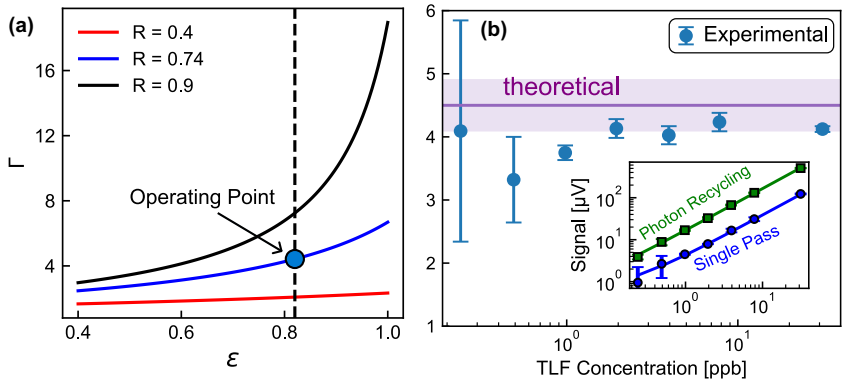

Fig. 2. (a) Enhancement factor (Γ) as per Eq. (8) at different geometric factors (ϵ) for $\rho = 10$ ppb. (b) Experimental Γ calculated from a serial dilution of tryptophan solution in photon-recycling (green squares) and single-pass (blue circles) sample chambers of lensless systems of the same geometry. The inset axis shows the raw detector signals for both system with ratio of slopes (photon recycling/single pass) of 4.3 ± 0.7.

<100 ppb tryptophan, we can assume the weak absorption limit:

$$\Gamma_{\epsilon,\rho\to 0} = \frac{(1+R)}{1-\epsilon R}. \tag{8}$$

The enhancement factor Γ calculated for various surface reflectivities and geometrical factors is shown in Fig. 2(a).

For a polished and protected aluminum surface, a typical reflectance value is $R \approx 0.92$ (at ∼276 nm [8]), resulting in a maximum possible enhancement factor of $\Gamma \approx 25$ [Fig. 2(b)]. We used Al-6061-T6 hand-polished to 320 grit (surface roughness of 36.5 μm giving negligible specular reflectivity, and dominant diffuse reflectivity) [9–11]. Based on the data provided by Hass *et al*. [11] for thick aluminum with oxidized surface ($83 \pm 3\%$ of non-oxidized aluminum), we estimate total reflectivity (dominated by diffuse reflections) of $76 \pm 3\%$. Incorporating bulk transmission of UV-grade synthetic quartz cuvette material of 99% (Fresnel reflections can be neglected as they contribute to the signal), we use $R = 74 \pm 3\%$. Our setup has a geometrical factor $\epsilon = 0.82 \pm 0.02$ (reflecting area $= 2090 \pm 70$ mm^2; area receiving flux $= 2552 \pm 70$ mm^2), which provides an enhancement factor of $\Gamma_\epsilon = 4.5 \pm 0.4$.

4. EXPERIMENTAL METHODS

The experimental setup [Fig. 1(d)] comprises a 275 nm UV LED excitation source (TUD7MF1B, SETi, Seoul Viosys), a synthetic UV grade quartz cuvette (CV10Q35F, Thorlabs) for holding water samples, and a silicon PIN photodetector (S1226-5BK, Hamamatsu Photonics 0.15 A/W photosensitivity at 350 nm) to collect the fluorescence signal. To ensure that sensitivity and surface effects of the photodetector are consistent across both setups, we utilize the same photodiode (and amplifier) in both setups. To isolate the weak fluorescence signal from the much stronger excitation light, a bandpass filter (Semrock FF01-356/30-25, 356 ± 15 nm) is positioned between the cuvette and the photodiode. The electrical current generated by the photodetector is then converted to a measurable voltage using a custom-built transimpedance amplifier, which is subsequently recorded by a data acquisition device.

In the single-pass sample chamber, the LED, cuvette, and photodiode are held in alignment by an enclosure fabricated from black polylactic acid (PLA) material using additive manufacturing. The black color was deliberately selected for its high absorbance, minimizing any stray reflections. In contrast, the photon-recycling sample chamber utilizes an enclosure made of Aluminum 6061, which reflects or scatters the excitation light back into the cuvette multiple times. Due to the significant light intensity enhancement achieved through these multiple reflections, we are able to operate the excitation LED at only 12.5% of its full optical power.

Experiments were conducted using L-tryptophan (Sigma Aldrich BCCC1787) solutions to compare the fluorescence sensitivity of the two chamber systems. A primary 200 ppm L-tryptophan stock solution was prepared by dissolving L-tryptophan powder in deionized (DI) water and stored at 4°C to maintain stability. The lower concentrations required for the experimental measurements were then prepared through serial dilution from this primary stock. All experiments were triplicated to ensure the consistency and reliability of the results.

5. EXPERIMENTAL RESULTS

Figure 2(b) illustrates Γ obtained experimentally by calculating the ratio of the fluorescence signal measured by the photodetector across a serial dilution of L-tryptophan solutions for both the photon-recycling and the single-pass chambers. Each data point on the inset plot represents the mean optical signal collected from the triplicate sets of the dilution experiments. The error bars correspond to one standard deviation from the mean, indicating the variance of the measurements. A linear fit was applied to the data to determine the sensitivity (slope) of each system to the L-tryptophan concentration.

The results demonstrate that the photon-recycling sample chamber significantly amplifies the fluorescence signal by a factor of 4.3 compared to the single-pass sample chamber. Furthermore, the reflective system exhibits a superior signal-to-noise ratio (SNR), especially at sub-parts-per-billion (ppb) TLF concentrations, confirming its enhanced performance in detecting trace levels of contamination. Also, note that the

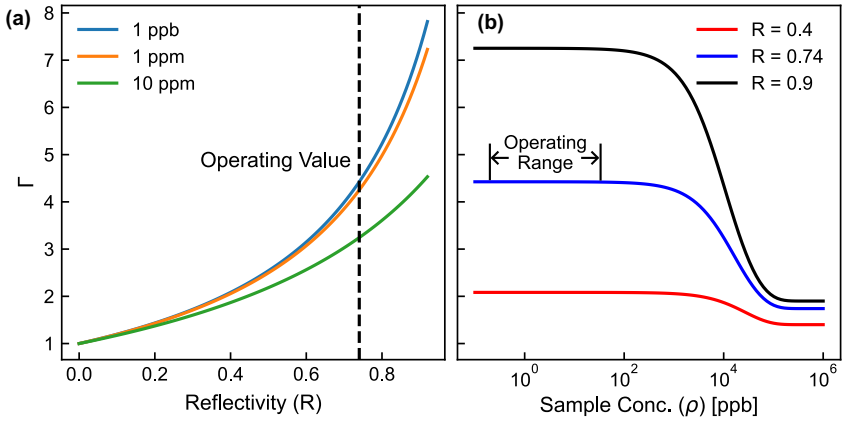

Fig. 3. Enhancement factor (Γ) as predicted by Eq. (7) for different values of (a) reflectivity (R) and (b) sample concentration (ρ) for tryptophan solution and single-pass interaction length $l_0 = 1$ cm.

experimentally observed enhancement factor lies within the error bounds of theoretical estimation.

6. DISCUSSION

We have successfully demonstrated a novel lensless fluorometer system incorporating a photon-recycling sample chamber that achieves a significant signal enhancement factor of approximately 4.3 compared to a conventional, non-reflective chamber within the same lensless geometry. Using the results of [4], this result can be extrapolated to obtain an 8× enhancement in the fluorescence signal compared to a typical fluorometer with lenses. This enhancement is attributed to the reflective aluminum enclosure, which causes the excitation light to undergo multiple passes and reflections inside the chamber. This multipass geometry effectively excites the sample volume several times, thereby amplifying the collected optical signal. In contrast, the single-pass (black PLA) chamber absorbs both excitation and emission signals emitted in the backward half-space, leading to much poorer photon utilization.

A key benefit of this signal amplification is the ability to operate the excitation source at significantly reduced power. We successfully decreased the LED's average drive current from 120 to 15 mA (at a 6 V forward voltage). This translates to a substantial reduction in power consumption, from 720 to 90 mW. The corresponding minimization of heat generation dramatically simplifies the system's thermal management requirements, eliminating the need for bulky heat sinks and facilitating the development of a smaller, more energy-efficient battery-powered device for handheld and remote water quality sensing. Our research utilizes the lensless setup described in Ref. [4] as the primary single-pass baseline. The observed performance gain is driven by the photon-recycling mechanism, which leverages the core "lensless" architecture to significantly improve miniaturization, integration, and overall system power efficiency.

A trade-off of the increased effective interaction length (or larger effective volume) achieved through photon recycling is the potential for enhanced quenching effects and non-linear performance at higher concentrations. In this research, we have only considered inner-filter effects [Eq. (4))] as the primary cause of non-linearity. Figures 3(a) and 3(b) illustrate the non-linearity as predicted by our model, which starts to appear at ≈ 1 ppm. For simplification purposes, we have assumed the absorptive system to be free of such inner filter effects, which further contributes to increasing at higher concentrations due to lower signal at such concentrations. Other quenching effects that are amplified by the reflective system (but not considered here) include quenching due to non-radiative energy transfer owing to increased path length and photobleaching, which is amplified as the sample receives greater excitation flux. We have concentrated our efforts primarily into detection of low concentrations of TLF, which are more important for drinking water applications. As a result, we have not observed such non-linear effects in our experiments (<31.25 ppb). Future work will involve quantifying these effects and developing compensation strategies.

The photon-recycling system demonstrated here is able to detect sub-ppb levels of tryptophan in water with high SNR. This high sensitivity, combined with the low power consumption and minimal heat generation, makes the platform particularly promising for quantifying microbial contamination in drinking water. The ability to utilize smaller components and reduce energy demand facilitates the development of a low-cost, miniaturized fluorometer [12] specifically suited for deployment in resource-limited settings and for continuous field monitoring.

Funding. Engineering and Physical Sciences Research Council (EP/P030017/1, EP/T020008/1, EP/W524165/1); Optica Foundation (Challenge Prize 2022, Challenge Prize 2024); World Academy of Sciences (18-013 RG/PHYS/AS_I, 21-334 RG/PHYS/AS_G, 22-244 RG/PHYS/AS_G); Fundação de Amparo à Pesquisa do Estado de São Paulo (2020/00619-4, 2021/06121-0); National Council for Scientific and Technological Development (307602/2021-4).

Disclosures. The authors declare no competing interests.

Data availability. Data relevant to the work presented in this paper are available from authors upon reasonable request.

REFERENCES

1. S. Cumberland, J. Bridgeman, A. Baker, *et al.*, "Fluorescence spectroscopy as a tool for determining microbial quality in potable water applications," Environ. Technol. **33**, 687–693 (2011).

2. J. P. Sorensen, J. Nayebare, A. F. Carr, *et al.*, "In-situ fluorescence spectroscopy is a more rapid and resilient indicator of faecal contamination risk in drinking water than faecal indicator organisms," Water Res. **206**, 117734 (2021).
3. A. Dahal, A. Thapa, R. Maharjan, *et al.*, "Autofluorescence spectroscopy meets UNICEF's target for water quality detection," Research Square (2025).
4. A. Maharjan, P. Waiba, S. Shrestha, *et al.*, "When a lensless fluorometer outperforms a lensed system," Optica **11**, 1124–1128 (2024).
5. T. Itoh, "Intensification of the emission signals using the reflection mirrors mounted to the sample holder of a fluorimeter," J. Fluoresc. **16**, 739–742 (2006).
6. N. Vekshin, "Multipass cuvettes for spectrofluorimetry," Anal. Chim. Acta **227**, 291–295 (1989).
7. C. N. Pace, F. Vajdos, L. Fee, *et al.*, "How to measure and predict the molar absorption coefficient of a protein," Protein Sci. **4**, 2411–2423 (1995).
8. X. Liu, Y. Mou, H. Wang, *et al.*, "Enhanced light extraction of deep ultraviolet light-emitting diodes by using optimized aluminum reflector," Appl. Opt. **57**, 7325–7328 (2018).
9. L. H. Li, N. H. Yu, C. Y. Chan, *et al.*, "Al6061 surface roughness and optical reflectance when machined by single point diamond turning at a low feed rate," PLoS One **13**, e0195083 (2018).
10. I. Lindseth, A. Bardal, and R. Spooren, "Reflectance measurements of aluminium surfaces using integrating spheres," Opt. Lasers Eng. **32**, 419–435 (1999).
11. G. Hass, W. R. Hunter, and R. Tousey, "Influence of purity, substrate temperature, and aging conditions on the extreme ultraviolet reflectance of evaporated aluminum," J. Opt. Soc. Am. **47**, 1070–1073 (1957).
12. P. Waiba, R. Bakhunchhe, A. Maharjan, *et al.*, "RealtimeWAS: a low-cost, portable device for real-time detection of fecal contamination in drinking water," in *Frontiers in Optics + Laser Science 2023 (FiO, LS)* (Optica Publishing Group, 2023), paper FM5G.3.